Electronic Supplementary Material (ESI) for Physical Chemistry Chemical Physics.

Supplementary Materials

Antiferromagnetic semiconducting $FeCN_2$ monolayer with a large magnetic anisotropy and strong magnetic coupling

Zhicui Wang,[a†] Huan Lou,[a,b†] Fanjunjie Han,[a,c] Xu Yan,[a] Yong Liu[*a] and Guochun Yang[*a]

[a]*State Key Laboratory of Metastable Materials Science & Technology and Key Laboratory for Microstructural Material Physics of Hebei Province, School of Science, Yanshan University, Qinhuangdao 066004, China.*
[b]*Department of Physics, College of Science, Jiangsu University of Science and Technology, Zhenjiang 212003, People's Republic of China.*
[c]*Centre for Advanced Optoelectronic Functional Materials Research and Key Laboratory for UV Light-Emitting Materials and Technology of Ministry of Education, Northeast Normal University, Changchun 130024, China.*

[†]Zhicui Wang and Huan Lou contributed equally to this work.
*Corresponding Authors E-mail:yongliu@ysu.edu.cn; yanggc@ysu.edu.cn.

Index **Page**

Computational Details

Our structural prediction approach is based on a global minimization of free energy surfaces merging ab initio total-energy calculations with CALYPSO (Crystal structure AnaLYsis by Particle Swarm Optimization) methodology as implemented in the CALYPSO code [1, 2]. The structures of stoichiometry $FeCN_2$ monolayer were searched with simulation cell sizes of 1-4 formula units (f.u.). In the first step, random structures with certain symmetry are constructed in which atomic coordinates are generated by the crystallographic symmetry operations. Local optimizations [3] using the VASP code were done with the conjugate gradients method and stopped when energy changes became smaller than 1×10^{-5} eV per cell. After processing the first generation structures, 60% of them with lower Gibbs free energies are selected to construct the next generation structures by PSO (Particle Swarm Optimization). 40% of the structures in the new generation are randomly generated. A structure fingerprinting technique of bond characterization matrix is applied to the generated structures, so that identical structures are strictly forbidden. These procedures significantly enhance the diversity of the structures, which is crucial for structural global search efficiency. In most cases, structural searching simulations for each calculation were stopped after generating 1000 ~ 1200 structures (e.g., about 20 ~ 30 generations).

To further analyze the structures with higher accuracy, we select a number of structures with lower enthalpies and perform structural optimization using density functional theory within the generalized gradient approximation [4] as implemented in the VASP code. The cut-off energy for the expansion of wavefunctions into plane waves is set to 500 eV in all calculations, and the Monkhorst–Pack k-mesh with a maximum spacing of $2\pi \times 0.03$ Å^{-1} was individually adjusted in reciprocal space with respect to the size of each computational cell. This usually gives total energies well converged within ~1 meV/atom. The electron-ion interaction was described by using all-electron projector augmented-wave method (PAW) with $3d^74s^1$, $2s^22p^3$, and $2s^22p^2$ considered as valence electrons for Fe, C, and N atom, respectively.

The cohesive energy E_{coh} is calculated according to the equation below:

$$E_{\mathrm{coh}} = (E_{FeCN_2} - E_{Fe} - E_C - 2E_N)/4 \qquad (1)$$

where E_{Fe}, E_C, E_N, and E_{FeCN_2} are the energies of the Fe atom, C atom, N atom, and $FeCN_2$ unit cell, respectively.

The Young's modulus $Y(\theta)$ and Poisson's ratio $v(\theta)$ along any direction θ (θ is the angle relative to the positive x-direction) are defined as

$$Y(\theta) = \frac{C_{11}C_{22} - {C_{12}}^2}{C_{11}s^4 + C_{22}c^4 + (\frac{C_{11}C_{22} - {C_{12}}^2}{C_{66}} - 2C_{12})c^2s^2} \quad (2)$$

$$v(\theta) = \frac{C_{12}(c^4 + s^4) - (C_{11} + C_{22} - \frac{C_{11}C_{22} - {C_{12}}^2}{C_{66}})c^2s^2}{C_{11}s^4 + C_{22}c^4 + (\frac{C_{11}C_{22} - {C_{12}}^2}{C_{66}} - 2C_{12})c^2s^2} \quad (3)$$

where c = $\cos\theta$ and s = $\sin\theta$.

Following the recipe of second-order perturbation theory proposed by *Wang et al*.,[5] the MAE of Fe atoms can be written as the following two terms

$$\Delta E^{--} = E^{--}(x) - E^{--}(z) = \xi^2 \sum_{o^-,u^-} \frac{\left|\left\langle o^- \middle| L_Z \middle| u^- \right\rangle\right|^2 - \left|\left\langle o^- \middle| L_x \middle| u^- \right\rangle\right|^2}{\varepsilon_{u}{}^{-} - \varepsilon_{o}{}^{-}} \quad (4)$$

$$\Delta E^{+-} = E^{+-}(x) - E^{+-}(z) = \xi^2 \sum_{o^+,u^-} \frac{\left|\left\langle o^+ \middle| L_Z \middle| u^- \right\rangle\right|^2 - \left|\left\langle o^+ \middle| L_x \middle| u^- \right\rangle\right|^2}{\varepsilon_{u}{}^{-} - \varepsilon_{o}{}^{+}} \quad (5)$$

Where ξ represents the SOC constant, $\varepsilon_u{}^-$ is the energy levels of unoccupied spin-down states $\left|u^-\right\rangle$, $\varepsilon_o{}^-$ and $\varepsilon_o{}^+$ are the energy levels of occupied spin-down states $\left\langle o^-\right|$ and occupied spin-up states $\left\langle o^+\right|$, respectively. Eqn (4) represents the contributions to magneto-crystalline anisotropy from the SOC interaction between occupied and unoccupied spin-down states, while Eqn (5) represents the contributions to magneto-crystalline anisotropy from the SOC interaction between occupied spin-up states and unoccupied spin-down states.

Supplementary Figures

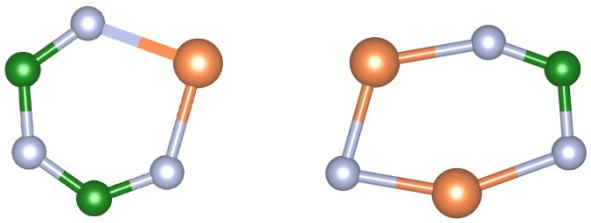

Fig. S1. Two different six-membered rings (i.e., FeC_2N_3 (left) and Fe_2CN_3 (right)) in the $FeCN_2$ monolayer.

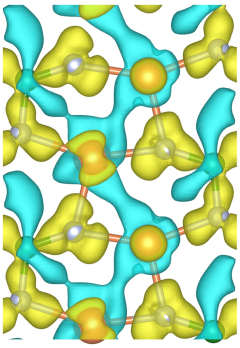

Fig. S2. Charge density difference of the $FeCN_2$ monolayer. The cyan part represents a decrease in charge density, and the yellow part represents an increase in charge density.

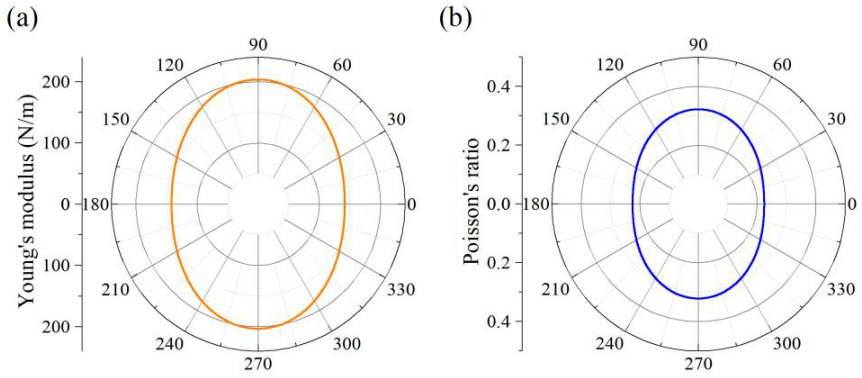

Fig. S3. Orientation-dependent in plane (a) Young's modulus $Y(\theta)$ and (b) Poisson's ratio $\nu(\theta)$ of the $FeCN_2$ monolayer.

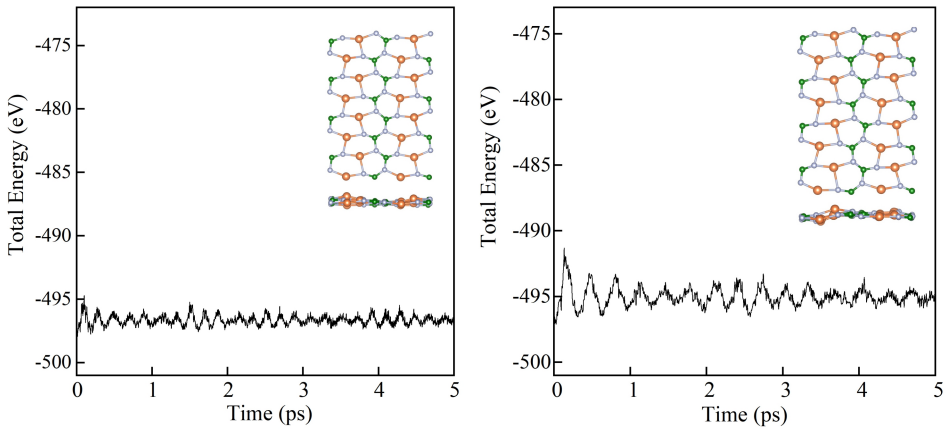

Fig. S4. Structure and total energy evolution for the $FeCN_2$ monolayer in AIMD simulation at 300 K (left) and 500 K (right).

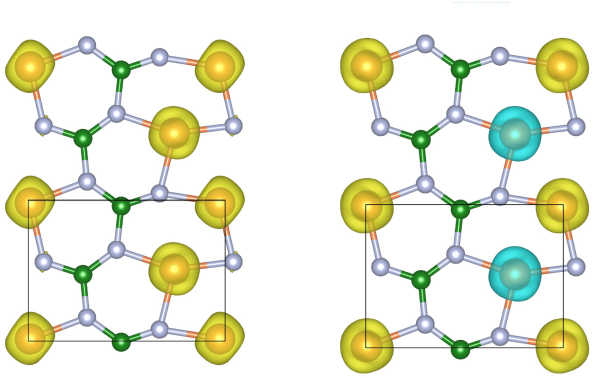

Fig. S5. Spin charge densities of FM, and AFM orders in $FeCN_2$ monolayer.

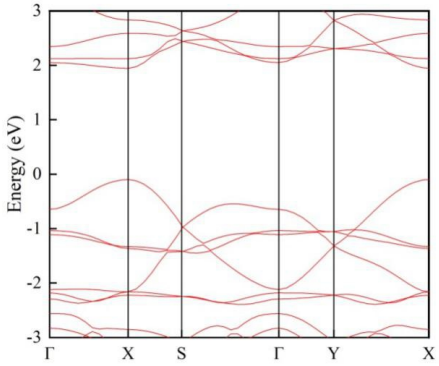

Fig. S6. The calculated band structure at HSE06 level of the $FeCN_2$ monolayer.

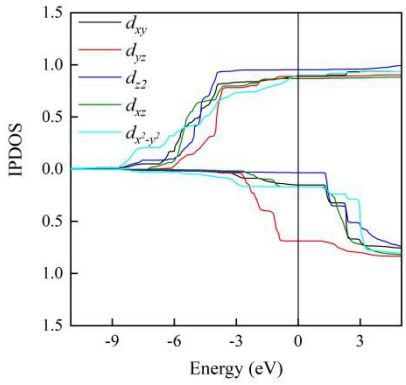

Fig. S7. The integrated PDOS of Fe atoms.

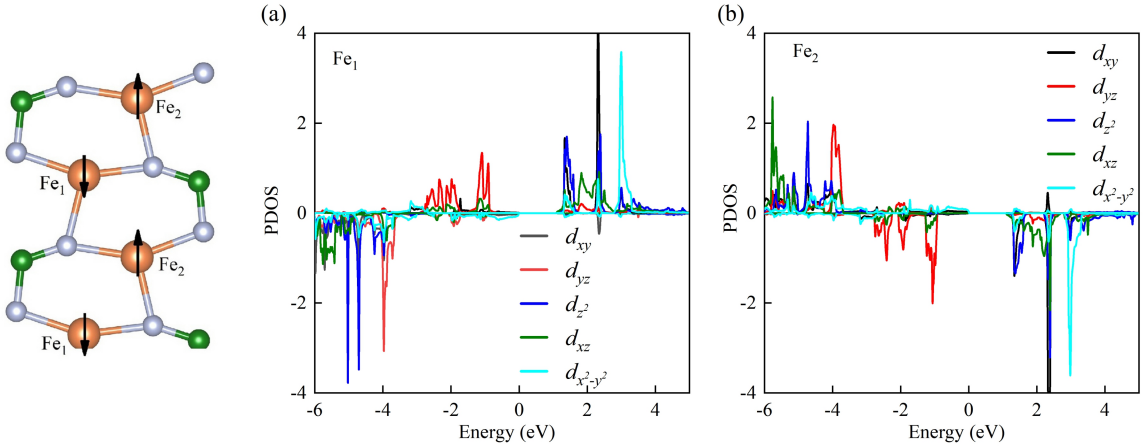

Fig. S8. (a) and (b) Projected density of states (PDOS) of 3*d* orbital for the nearest neighbor Fe atoms.

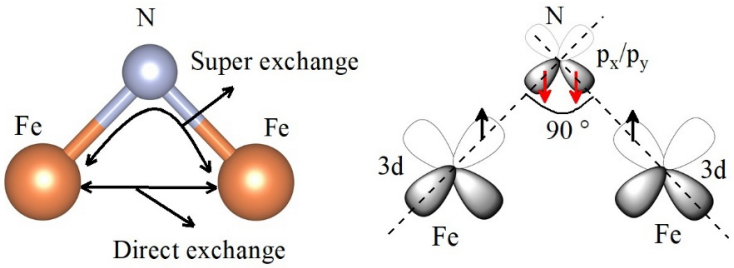

Fig. S9. Schematic illustration of the mechanisms of the direct exchange (Fe-Fe) and the super exchange (Fe-N-Fe) interaction. The relative positions of the 2*p* orbitals in the N atom and the 3*d* orbitals in the Fe atoms in the $FeCN_2$ monolayer.

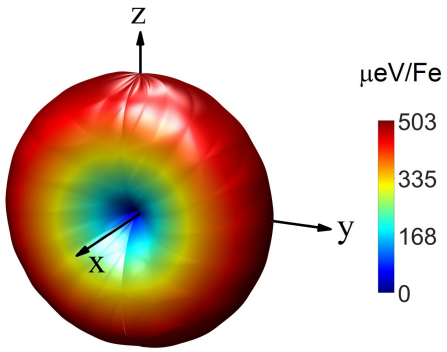

Fig. S10. MAE in 3D space of the $FeCN_2$ monolayer.

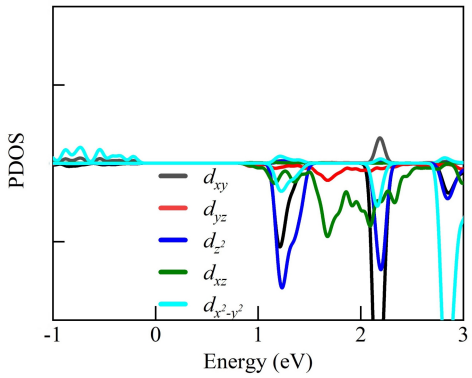

Fig. S11. PDOS of 3d orbital of Fe atom near the Fermi level.

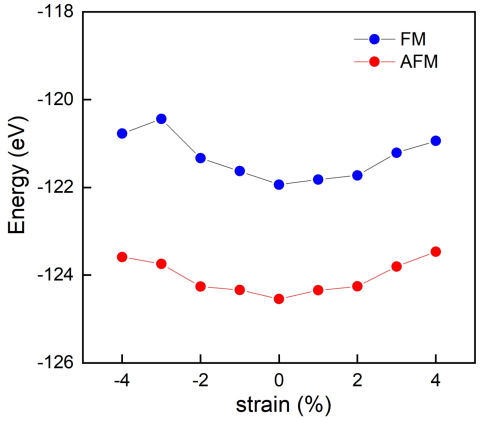

Fig. S12. The total energies of FM, and AFM orders for 1 × 2 × 1 super cell under biaxial strains.

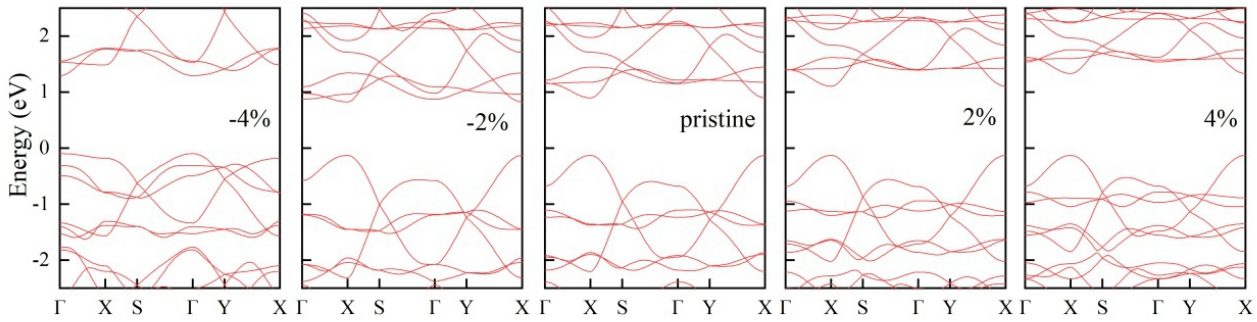

Fig. S13. The energy band (GGA + U) structure under biaxial strains of the $FeCN_2$ monolayer.

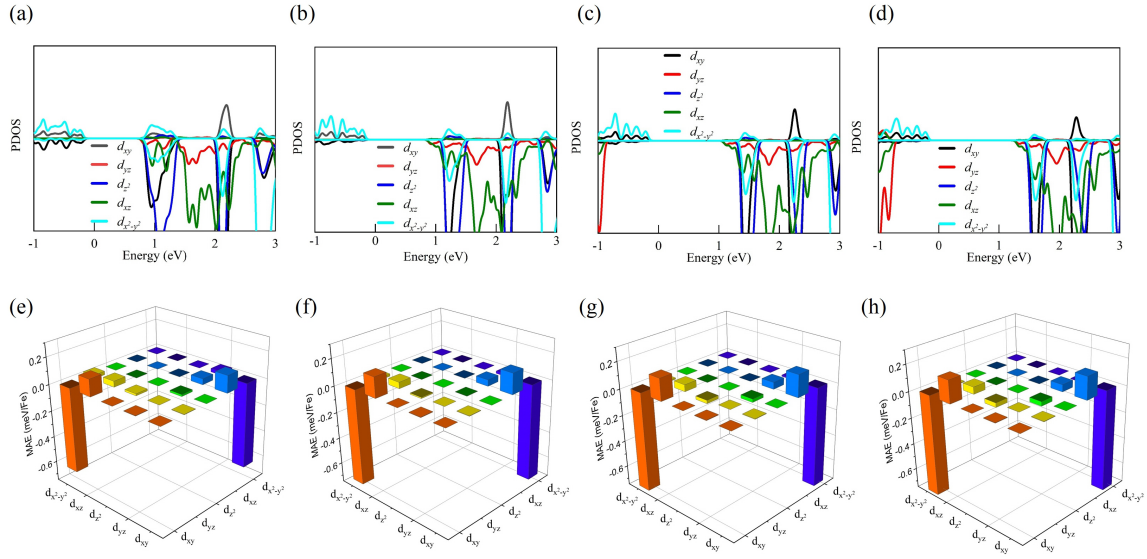

Fig. S14. (a-d) PDOS and (e-h) orbital-projected contribution to MAE from the SOC interaction for Fe atom in the $FeCN_2$ monolayer under -2% , pristine, 2%, and 4% biaxial strain, respectively.

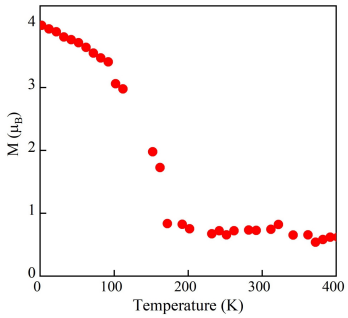

Fig. S15. Magnetic moment of Fe atoms versus temperature in the $FeCN_2$ monolayer under -3% biaxial strain.

Supplementary Tables

Table S1. The detailed structural information of the predicted stable $FeCN_2$ monolayer.

Lattice	**Wyckoff Positions (fractional)**			
Parameter(Å, °)	**Atoms**	***x***	***y***	***z***
a = 6.1668	Fe (1a)	0.38744	0.07450	0.50000
b = 4.4095	Fe(1a)	0.61256	0.57450	0.50000
	N1(1a)	0.91871	0.72814	0.50000
a = 90.0000	N2 (1a)	0.08129	0.22814	0.50000
β = 90.0000	N3(1a)	0.69824	0.14895	0.50000
γ = 90.0000	N4(1a)	0.30176	0.64895	0.50000
	C1(1a)	0.09929	0.54837	0.50000
	C2(1a)	0.90071	0.04837	0.50000

Table S2. Elastic coefficients C_{ij}, Young's modulus E, and Poisson's ratio v of $FeCN_2$ monolayer.

C_{11} (N/m)	C_{12} (N/m)	C_{22} (N/m)	C_{66} (N/m)	E_{min} (N/m)	E_{max} (N/m)	v_{min}	v_{max}
152.71	49.15	219.28	65.83	141.69	203.45	0.22	0.32

Table S3. The difference of square of the orbital angular momentum matrix elements between two directions of the magnetization in Eqn (5) $\left(\left|\left\langle o^{+}\left|L_x\right|u^{-}\right\rangle\right|^2-\left|\left\langle o^{+}\left|L_z\right|u^{-}\right\rangle\right|^2\right)$

	u$^-$				
o$^+$	d_{xy}	d_{yz}	d_{z2}	d_{xz}	d_{x2-y2}
d_{xy}	0	0	0	1	-4
d_{yz}	0	0	3	-1	1
d_{z2}	0	3	0	0	0
d_{xz}	1	-1	0	0	0
d_{x2-y2}	-4	1	0	0	0

Table S4. Band Gap at GGA+U level, magnetic moments per Fe (M), magneto-crystalline anisotropic energy (MAE), Fe-N and Fe-Fe bond lengths, Fe-N-Fe bond angle (°), magnetic exchange coupling parameters (J) of the $FeCN_2$ monolayer under biaxial strains from -4% to 4%.

Biaxial Strain (%)	**Gap (eV)**	M_{Fe} (μ_B)	**MAE (meV/Fe)**	**Bond length (Å)**		**Bond angle (°)**	J **(meV)**
				Fe-Fe	**Fe-N**	**Fe-N-Fe**	
-4%	1.49	2.59	0.25	2.44	1.81	83.81	-73.44
-3%	0.96	3.20	0.33	2.46	1.86	83.36	-103.14
-2%	0.95	3.34	0.45	2.51	1.89	83.62	-90.84
-1%	0.95	3.46	0.47	2.56	1.92	83.91	-84.59
0	1.03	3.50	0.50	2.60	1.94	83.99	-81.00
1%	1.14	3.55	0.54	2.64	1.97	84.03	-78.96
2%	1.23	3.57	0.55	2.68	2.00	84.05	-79.00
3%	1.36	3.60	0.56	2.71	2.04	84.06	-81.09
4%	1.46	3.61	0.57	2.75	2.07	84.11	-79.34

References

[1] Y. Wang, J. Lv, L. Zhu and Y. Ma, Phys. Rev. B **82**, 094116 (2010).

[2] Y. Wang, J. Lv, L. Zhu and Y. Ma, Comput. Phys. Commun. **183**, 2063 (2012).

[3] G. Kresse and J. Furthmüller, Phys. Rev. B **54**, 11169 (1996).

[4] Matteo Cococcioni and Stefano de Gironcoli, Phys. Rev. B **71**, 035105 (2005).

[5] D.-S. Wang, R. Wu, and A. J. Freeman, Phys. Rev. B **47**, 14932(1993).